Precision Measurement of the ^{29}Si, ^{33}S, and ^{36}Cl Binding Energies

M. S. Dewey,* E. G. Kessler, Jr.,† and R.D. Deslattes‡
National Institute of Standards and Technology
Gaithersburg, MD 20899

H.G. Börner, M. Jentschel, C. Doll, and P. Mutti
Institut Laue-Langevin, F-38042 Grenoble CEDEX, France
(Dated: February 8, 2008)

The binding energies of ^{29}Si, ^{33}S, and ^{36}Cl have been measured with a relative uncertainty $< 0.59 \times 10^{-6}$ using a flat-crystal spectrometer. The unique features of these measurements are 1) nearly perfect crystals whose lattice spacing is known in meters, 2) a highly precise angle scale that is derived from first principles, and 3) a gamma-ray measurement facility that is coupled to a high flux reactor with near-core source capability. The binding energy is obtained by measuring all gamma-rays in a cascade scheme connecting the capture and ground states. The measurements require the extension of precision flat-crystal diffraction techniques to the 5 to 6 MeV energy region, a significant precision measurement challenge. The binding energies determined from these gamma-ray measurements are consistent with recent highly accurate atomic mass measurements within a relative uncertainty of 4.3×10^{-7}. The gamma-ray measurement uncertainties are the dominant contributors to the uncertainty of this consistency test. The measured gamma-ray energies are in agreement with earlier precision gamma-ray measurements.

arXiv:nucl-ex/0507011v1 6 Jul 2005

I. INTRODUCTION

Nuclear binding energy measurements are of interest because they are accurately related to atomic mass measurements. This relationship provides a means to check the results in one precision measurement field against related results obtained in another precision measurement field. Because the experimental techniques used in the two fields are very different, this check has the potential to reveal systematic errors associated with either measurement.

The synergism between binding energy and atomic mass measurements can be demonstrated by considering a typical neutron capture reaction $n + {}^{A}\mathrm{X} \rightarrow {}^{A+1}\mathrm{X} + \gamma$'s which leads to the following equation involving atomic masses and the binding energy,

$$m(n) + m({}^{A}\mathrm{X}) = m({}^{A+1}\mathrm{X}) + S_n \,. \qquad (1)$$

Atomic masses m are measured in atomic mass units while the binding energy of ${}^{A+1}$X, S_n, is obtained from gamma-ray wavelengths measured in meters. The binding energy in meters can be converted to atomic mass units using the molar Planck constant, $N_A h$, divided by the speed of light, c [1]. This combination of constants is known with a relative uncertainty of 6.7×10^{-9}, an accuracy which does not limit the test implied by Eq. (1), given the presently available accuracy in atomic mass and binding energy measurements [2].

New precision measurements of the ^{29}Si, ^{33}S, and ^{36}Cl binding energies have been made using a flat crystal spectrometer. This spectrometer measures the wavelengths of the gamma-ray photons using crystals whose lattice spacings are known in meters and an angle scale that is derived from first principles. Thus, the measured wavelengths are on a scale consistent with optical wavelengths and the SI definition of the meter. The binding energies of these three nuclei are in the 8.5 to 8.6 MeV range and are obtained by measuring lower energy lines that form a cascade scheme connecting the capture and ground states. For all three nuclei, the cascade scheme with the most intense transitions includes a gamma-ray with energy $> 4.9\,$MeV. Such high energies present a significant measurement challenge for gamma-ray spectroscopy because the Bragg angles are $< 0.1^\circ$ and the diffracted intensity is rather small (a few s^{-1} or less).

II. THE ^{29}SI, ^{33}S, AND ^{36}CL DECAY SCHEMES

In Fig. 1 we show partial decay schemes for ^{29}Si, ^{33}S, and ^{36}Cl containing the transitions that were measured in these binding energy determinations. The values in parentheses are the number of gamma-rays emitted per 100 captures [3]. The reactions, the thermal neutron capture cross sections, and the nominal energies of the measured gamma-rays are listed in Table I [4]. Because ^{35}Cl has the largest thermal neutron capture cross section of any light nuclei, the ^{36}Cl binding energy was measured first. The experience gained in increasing the crystal reflectivity and lowering the background during the ^{36}Cl measurement proved to be very valuable in the measurement of the weaker ^{29}Si and ^{33}S transition energies. In addition, a larger than expected dependence of the angle calibration on the environment was noted during the Cl measurements which led to more frequent angle calibrations during the ^{29}Si and ^{33}S measurements. The ^{29}Si

*Electronic address: maynard.dewey@nist.gov
†Electronic address: ernest.kessler@nist.gov
‡Deceased

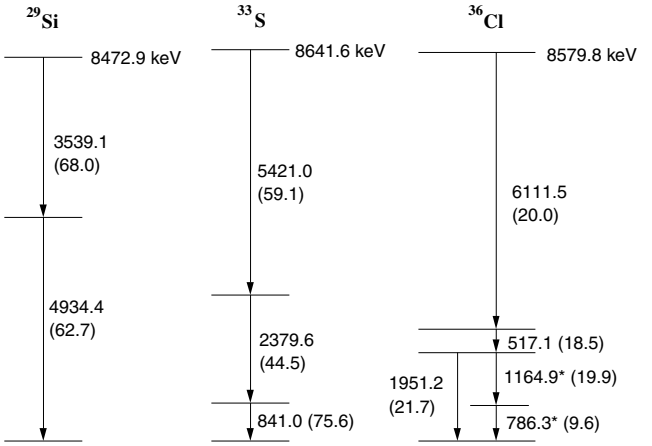

FIG. 1: Partial decay schemes for ^{29}Si, ^{33}S, ^{36}Cl showing the transitions that were measured in this study. The numbers in parentheses are the number of gammas per 100 neutron captures. The transitions marked with asterisks in Cl were not used to deduce binding energies.

measurement is particularly difficult because the 4934 keV line is emitted while the nucleus is recoiling following the emission of the 3539 keV line. Thus, the 4934 keV profile is significantly Doppler broadened which decreases the accuracy with which the Bragg angle can be determined. In each of these nuclei there are other less intense transitions that connect the capture and ground states. However, the measurement uncertainty of these weaker lines will be so large that their contribution to the binding energy determination will be small. As the stability of the spectrometer improves and techniques to measure weaker lines are developed, these weaker lines may be used for future binding energy determinations.

III. EXPERIMENT

The measurements were made at the Institut Laue-Langevin (ILL) using the GAMS4 flat crystal spectrometer. A detailed description of this facility is available to the interested reader in Ref. 5. The discussion of the experiment given here will be limited to those aspects that are peculiar to these measurements. This spectrometer is located on the reactor floor at the exit of a through-tube that has facilities to transport and hold sources next to the reactor core. Five beamtime allocations were devoted to these binding energy measurements. Chlorine was measured in February 1997 and September 1997. Sulfur was measured in September–October 1998 and April–May 1999. Silicon was measured in October–November 2000. The first measurement cycle (February 1997) served as a proof of the capability of the facility to determine binding energies. In retrospect, it was necessary to exclude all data taken during this cycle from the final results because the experimental conditions were not sufficiently controlled.

The stability of the angle calibration of the spectrometer has been a particularly troublesome experimental problem. Throughout the extended period of the measurements reported here, the angle calibration of the spectrometer has been measured many times, both during and between the binding energy measurements. However, at the start of these measurements we were not aware of the dependence of the angle calibration on the humidity and did not perform calibrations as frequently. From 1998 forward, more frequent calibrations have provided a means to obtain more accurate angle calibrations. Following considerable data analyses aimed at mining the angle calibrations and gamma-ray measurements for maximum information, we have reached the following conclusions concerning the angle calibration: a relative uncertainty due to the angle calibration of $\approx 0.4 \times 10^{-6}$ should be included in each measurement period. More details concerning the angle calibration are given in Sec. IV.

At the start of the experiment, it was our intention to measure the 786 keV and 1165 keV lines in Cl to provide a cascade cross-over verification of the 1951 keV line. Because of beamtime restrictions and angle calibration difficulties, this cascade cross-over verification was not realized. However, a very limited data set for the 786 keV line was recorded and used to provide a value for the wavelength of this transition.

A. Sources

The source handling mechanism can accommodate three sources that are positioned one behind the other on the beam axis, a line connecting the source region and the center of the axis of rotation of the first crystal. The source material was placed in thin-walled graphite holders that are supported on "V"s for precise positioning. Two sizes of graphite holders were used. For the two chlorine and first sulfur measurements, the inside volume of the source holder was 2 mm × 50 mm × 25 mm with the 2 mm × 50 mm surface facing the spectrometer. For the second sulfur and silicon measurement, the inside volume was 3.5 mm × 50 mm × 25 mm with the 3.5 mm × 50 mm surface facing the spectrometer. The neutron flux at the source position is $\approx 5.5 \times 10^{14}$ cm^{-2} s^{-1}. In Table II the sources, the source masses, and the estimated activities for each of the measurements are given. The sources that are used are extremely active to compensate for the small effective solid angle (high resolution) of the spectrometer.

B. Spectrometer

The critical component of the gamma-ray facility is a double flat crystal spectrometer that has three unique capabilities that are very important for the accurate measurement of pico-meter wavelengths. First, the diffrac-

TABLE I: Reactions, cross-sections, and nominal energies associated with the binding energy determinations.

Nuclide	Reaction	Cross-section ($\times 10^{-28}$ m^2)	Nominal binding energy (keV)	Energies measured (keV)
^{29}Si	$n + {}^{28}\mathrm{Si} \rightarrow {}^{29}\mathrm{Si} + \gamma$	0.177	8473	3539, 4934
^{33}S	$n + {}^{32}\mathrm{S} \rightarrow {}^{33}\mathrm{S} + \gamma$	0.53	8642	841, 2380, 5421
^{36}Cl	$n + {}^{35}\mathrm{Cl} \rightarrow {}^{36}\mathrm{Cl} + \gamma$	43.6	8580	517, 786, 1951, 6112

TABLE II: Sources, source masses, and estimated activities for each of the measurements.

Nuclide	Measurement dates	Source	Source mass (g)	Estimated activity ($\times$ 10^{13} Bq)
^{29}Si	Oct–Nov 2000	Si single crystal	13.4	2.6
^{33}S	Sept–Oct 1998	ZnS single crystal	8.1	1.4
^{33}S	April–May 1999	ZnS polycrystal	16.8	2.9
^{36}Cl	Feb 1997	NaCl	4.5	85.4
^{36}Cl	Sept 1997	NaCl	4.5	85.4

tion crystals are highly perfect specimens whose lattice spacing is measured on a scale consistent with the SI definition of the meter. Second, the diffraction angles are measured with sensitive Michelson angle interferometers which are calibrated using an optical polygon [5]. The angle calibration is based on the fact that the sum of the external angles of the polygon equals 360°. Third, the gamma-ray beam collimation is sufficient to permit the measurement of very small diffraction angles ($< 0.05°$). The GAMS4 facility is a precision metrology laboratory with the usual attention to vibration isolation, temperature control, and environmental monitoring.

Because descriptions of the profile recording and the angle calibration that follow assume some knowledge of the angle measuring system of the spectrometer, a few details concerning the angle interferometers are provided. Each of the two Michelson angle interferometers contains two corner cube retro-reflectors that are rigidly attached to the crystal rotation table. As the crystal rotates, the path length of one arm of the interferometer increases while the path length of the other arm decreases. The angles are measured in whole and fractional interferometer fringes with 1 fringe $\approx 7.8 \times 10^{-7}$ rad. An interferometer fringe can be divided into ≈ 1000 parts ($\approx 7.8 \times 10^{-10}$ rad). The arm that supports the retro-reflectors is made out of low expansion invar in order to reduce the temperature dependence of the angle interferometer. Nevertheless, the temperature of the corner cube arm must be taken into account when converting interferometer fringe values into angles (see Sec. IV). Because the interferometers are in the laboratory environment, all angle fringe measurements must be corrected to standard pressure, temperature, and humidity conditions.

C. Crystals

The gamma-rays measured in this study were diffracted by nearly perfect silicon crystals used in transmission geometry. All of the crystals were cut so that the (220) family of planes was available for diffraction and have a shape and mounting identical to the crystal shown in Fig. 7, Ref. 5. Because of the large spread in energy of the gamma-rays, two different sets of crystals were used. The first set, called ILL2.5, consisted of two crystals of nearly equal thickness ($\approx$ 2.5 mm), and are the same crystals used for the measurement of the deuteron binding energy [6]. The raw material for these crystals was obtained from the Solar Energy Research Institute [7]. The second set, called ILL4.4&6.9, consisted of two crystals of unequal thickness ($\approx$ 4.41 mm and $\approx$ 6.95 mm) manufactured from raw material obtained from Wacker [7]. The ILL2.5 crystals were used for the lower energy lines (S 841 keV and 2380 keV and the Cl 517 keV, 786 keV, and 1951 keV lines) and initial measurements of the Cl 6111 keV line. The ILL4.4&6.9 crystals were used for the higher energy lines (Si 3539 keV and 4934 keV, S 5421 keV, and Cl 6111 keV lines). The dependence of integrated reflectivity on crystal thickness and energy is discussed in more detail in Section 11, Ref. 5. Each line was measured in at least two orders that were chosen on the basis of high reflectivity and small diffraction width. In Table III the crystal configurations that were used for each energy are given along with the nominal Bragg angles.

In the past our approach to the determination of the unknown lattice spacing of diffraction crystals combined two types of crystal lattice spacing measurements: 1) absolute lattice parameter measurements in which the lattice parameter of a particular Si crystal is compared to

TABLE III: Crystals, crystal orders, and nominal Bragg angles for the various energies.

Nuclide	Energy	Crystals	A crystal		B crystal	
	(keV)		order-m	Bragg angle°	order-n	Bragg angle°
^{29}Si	3539	ILL4.4&6.9	1	0.052	2,-2	0.105
	3539	ILL4.4&6.9	1	0.052	3,-3	0.157
	4934	ILL4.4&6.9	1	0.037	1	0.037
	4934	ILL4.4&6.9	1	0.037	2,-2	0.075
^{33}S	841	ILL2.5	1	0.220	1,-1	0.220
	841	ILL2.5	1	0.220	3,-3	0.660
	2380	ILL2.5	1	0.078	1	0.078
	2380	ILL2.5	1	0.078	2,-2	0.155
	2380	ILL2.5	1	0.078	-3	0.233
	5421	ILL4.4&6.9	1	0.034	1	0.034
	5421	ILL4.4&6.9	1	0.034	2,-2	0.068
	5421	ILL4.4&6.9	1	0.034	3,-3	0.102
^{36}Cl	517	ILL2.5	2	0.716	2,-2	0.716
	517	ILL2.5	2	0.716	3,-3	1.074
	786	ILL2.5	1	0.235	1,-1	0.235
	1951	ILL2.5	1	0.095	2,-2	0.190
	1951	ILL2.5	2	0.190	2,-2	0.190
	6111	ILL2.5, ILL4.4&6.9	1	0.030	1	0.030
	6111	ILL2.5, ILL4.4&6.9	1	0.030	2	0.061
	6111	ILL2.5, ILL4.4&6.9	1	0.030	3,-3	0.091

the wavelength of an $^{127}I_2$ stabilized laser and 2) lattice comparison (relative) measurements in which the small lattice spacing difference between known and unknown crystal samples was measured. Absolute lattice parameter measurements have been published by researchers at the Physikalisch-Technische Bundesanstalt (PTB) in 1981 [8], at the Istituto di Metrologia "G. Colonnetti" (IMGC) in 1994 [9], and at the National Measurement Institute of Japan (NMIJ) in 1997 [10]. Lattice comparison measurements have been made at the PTB [11] and the National Institute of Standards and Technology (NIST) [12, 13]. In Ref. 6 the above approach applied to the determination of the lattice parameter of the ILL2.5 crystals is described in detail using the data that was available in 1999. Although an early 2004 publication contains improved absolute lattice parameter measurements from IMGC and NMIJ [14], the authors have since published an erratum and advised us not to use these results [15].

One of the authors of the 1998 and 2002 CODATA Recommended Values of the Fundamental Physical Constants has recommended an alternate approach for determining lattice parameters values for the crystals used in these measurements [16]. In the adjustment of the fundamental physical constants, absolute and relative lattice parameter measurements are used in a consistent way to arrive at recommended output values. One of the output values is the lattice parameter of an ideal single crystal of naturally occurring Si free of impurities and imperfections. Since the relative lattice parameter measurements connecting the ILL2.5 crystals to the PTB, IMGC, and NMIJ absolute lattice parameter crystals in Ref. 6 are included in the input data, the value of the lattice parameter of the ILL2.5 crystal is an unpublished output of the adjustment process. In the 2002 CODATA adjustment [2] only the NMIJ absolute lattice parameter value was used as input based on preliminary measurements that were eventually published in Ref. 14. Because these measurements are now known to be in error, the best estimate for the lattice parameter of the ILL2.5 crystal must be taken from the 1998 CODATA adjustment [17] and is d(220) ILL2.5 = 1.920155822(57)$\times 10^{-10}$ m at ϑ = 22.5 °C in vacuum (relative uncertainty of 3.0×10^{-8}). We prefer to arbitrarily increase the relative uncertainty to 5.0×10^{-8} to account for the present inconsistency of absolute and relative lattice parameter results and the variation of the lattice spacing within the raw material from which the crystals are manufactured.

To obtain a value for the lattice parameter of the ILL4.4&6.9 crystal, the NIST lattice comparison facility was used to measure the lattice spacing difference between the ILL2.5 and ILL4.4&6.9 crystals. The directly measured relative lattice parameter difference is $(\text{ILL2.5} - \text{ILL4.4\&6.9})/\text{ILL2.5} = 4.0 \times 10^{-8}$. By combining this relative lattice parameter measurement with the above absolute value for d(220) ILL2.5 yields the value for d(220) ILL4.4&6.9 that is given in Table IV. The reasons for preferring this approach for determining lattice parameter values over the approach that was used in Ref. 6 are all lattice parameter measurements included in

TABLE IV: Lattice spacing of ILL2.5 and ILL4.4&6.9 crystals. The ILL2.5 value is an unpublished output of the CODATA adjustment process. The NIST lattice comparison facility was used to measure the lattice spacing difference between the ILL2.5 and ILL4.4&6.9 crystals.

$d(220)^a$ ILL2.5 (m)	$1.920155822(96) \times 10^{-10}$
(ILL2.5 − ILL4.4&6.9)/ILL2.5	$4.0(1.0) \times 10^{-8}$
$d(220)^a$ ILL4.4&6.9 (m)	$1.920155745(96) \times 10^{-10}$

$^a\vartheta = 22.5$ °C, in vacuum

the 1998 CODATA adjustment are used in a consistent way to obtain a value for d(220) ILL2.5 and only one direct lattice comparison is needed to obtain a value for d(220) ILL4.4&6.9.

However, it is instructive to compare the d(220) values given in Table IV to d(220) values obtained with the procedure used in Ref. 6. The relative difference between the values for d(220) ILL2.5 given in Table IV and in Ref. 6 is 5.2×10^{-8}. The deuteron binding energy and the neutron mass values given in Ref. 6 must be corrected for this change. In order to use the Ref. 6 approach to determine the ILL4.4&6.9 lattice spacing, the ILL 4.4&6.9 crystal was compared to the absolute lattice parameter crystals from PTB, IMGC, and NMIJ. The relative difference between the value for d(220) ILL4.4&6.9 given in Table IV and the value that is obtained using the Ref. 6 procedure is 3.9×10^{-8}. These relative differences provide further justification for expanding the relative uncertainty of the lattice parameter measurements to 5×10^{-8}. In addition, the lattice parameter difference between the ILL2.5 and ILL4.4&6.9 crystals can be inferred from the two d(220) values obtained with the Ref. 6 approach. The implied value of $(\text{ILL2.5} - \text{ILL4.4\&6.9})/\text{ILL2.5} = 3.0 \times 10^{-8}$ agrees very well with the directly measured value given above and provides further confidence in the lattice parameter results that are used to obtain binding energy measurements.

D. Profile recording

Gamma-ray profiles (intensity vs interferometer fringes) were recorded for the crystal configurations given in Table III by scanning the angular position of the second crystal. The profiles consisted of 30 to 45 points with counting times from 30 to 180 seconds per point and were scanned in both the cw and ccw directions. For each data point the interferometer fringe value was reduced to standard atmospheric conditions (pressure, temperature, and humidity) [18, 19]. The gamma-ray counts were accumulated in a Ge detector-multichannel analyzer system. The recorded profiles were least squares fit to theoretical dynamical diffraction profiles broadened with a Gaussian function to account for crystal imperfections, vibrations, and thermal and recoil induced motions of the atoms in the source. The use of a single Gaussian function to account for deviations of the recorded profiles from the theoretical dynamical diffraction profiles has been shown to provide reliable peak positions, but is not sufficient to obtain nuclear level lifetimes and recoil velocities from profile width measurements [20]. The adjustable parameters in the fit are the position, intensity, background, and Gaussian width contribution. In the fit, the number of counts at fringe value i, n_i, is weighted by $(1/\sqrt{n_i})^2$. The detector and fitting procedure are described in more detail in Ref. 5. Two representative profiles are shown in Fig. 2. The profile positions (in interferometer fringes), the most important parameter for the determination of energies, are converted into diffraction angles by using the second-axis angle calibration that is described in the next section.

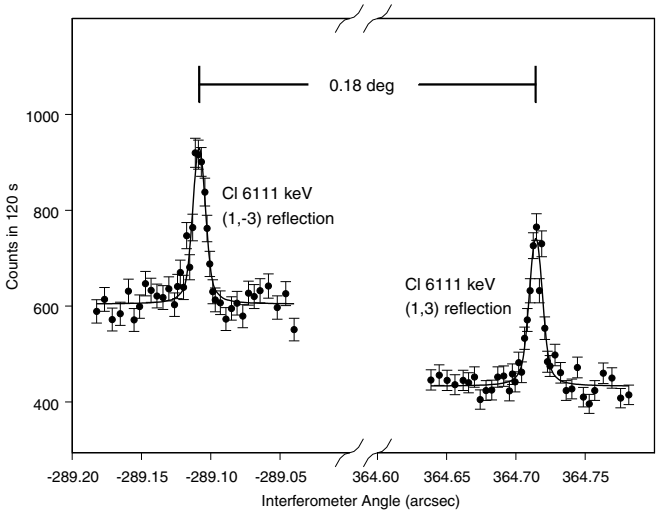

FIG. 2: Two representative third order ^{36}Cl profiles along with fitted curves: 6111 keV (1,-3) and (1,3) made with the thick crystals ILL4.4&6.9. The most important fit parameter is the profile centroid. The difference in profile centroids is proportional to the Bragg angle while the numeric mean of the two centroids gives the offset angle between the second crystal diffracting planes and the angle interferometer.

IV. ANGLE INTERFEROMETER CALIBRATION

A complete description of a calibration run can be found in Ref. 5. As discussed there the formula connecting optical fringes f, which are recorded with the rocking curves, and the true interferometer angle θ is

$$f = K \sin\theta + f_0 \,, \tag{2}$$

where K is the instrument calibration constant and f_0 is an electronic offset. Both terms must be determined experimentally through a calibration procedure. Ideally K would be invariable, however experience shows that K

depends on temperature, time, humidity and interferometer laser and alignment.

A. The Global Calibration Procedure

Between September 1997 and May 2002, a period spanning the measurements described in this paper, the GAMS4 spectrometer was calibrated 29 times. Table V lists each of these calibrations. The experimentally determined calibration constants (column 5) fit well to a linearized equation

$$K = K_0 + K_\vartheta(\vartheta - 26) + K_d(d - 800) + K_h(h - 0.35) + K_{\rm laser} \times \begin{cases} -1 & \text{if } d < 700, \\ 1 & \text{if } d > 700 \end{cases} \quad (3)$$

where $K = K(\vartheta, d, h)$ is the desired calibration constant, ϑ is the corner cube arm temperature (°C), h is the relative humidity, d is the number of days after 8/31/1997, and $d = 700$ corresponds to 8/1/1999 when the interferometer laser was replaced. A least squares fit to the data in Table V gives

$$\begin{aligned} K_0 &= 5133462.12 \pm 0.59 \\ K_\vartheta &= 7.5 \pm 1.3 \ /^\circ\text{C} \\ K_d &= -0.0059 \pm 0.0013 \\ K_h &= 41.6 \pm 3.9 \\ K_{\rm laser} &= 3.13 \pm 0.57 \end{aligned} \quad (4)$$

where $\vartheta_{\rm avg} = 26$ °C, $h_{\rm avg} = 0.35$, and $d_{\rm avg} = 800$ (11/9/1999) are average conditions around which the fit is made. This fit is plotted in Fig. 3. The relative standard deviation of the residuals (column 7) is 0.33×10^{-6}. Eqs. (2), (3), and (4) along with values for the profile centroid in fringes, the mean corner cube arm temperature, the mean humidity, and the mean wall time can be used to extract a profile centroid in radians from a single data file. This procedure uses all available calibration data to determine one set of coefficients $(K_0, K_\vartheta, K_d, K_h, K_{\rm laser})$ that are assumed valid for all of the data presented in this paper. In the remainder of this paper this procedure is referred to as the Global Calibration.

The dependence of K on temperature and time is not unexpected as the physical dimensions of the interferometer corner cube arm can vary with temperature and time in roughly the amounts seen [21, 22]. The data reveals no dependence of K on atmospheric pressure which is as expected since the interferometer fringe values are reduced to standard atmospheric conditions and the small pressure changes are not likely to alter the dimensions of the interferometer. The relative magnitude of the dependence on interferometer laser ($\approx 1.22 \times 10^{-6}$) is somewhat larger than the expected variability in the laser wavelength and is likely due to interferometer alignment. The dependence of K on humidity is unexpected and no definitive cause has been established. In an effort to better understand the dependence of the calibration on the environment, more frequent calibrations were performed as the measurements progressed. As is evident from Fig. 3, there are significant differences between some values of $K_{\rm measured}$ and $K_{\rm fit}$. These differences prompted us to consider alternate calibration procedures.

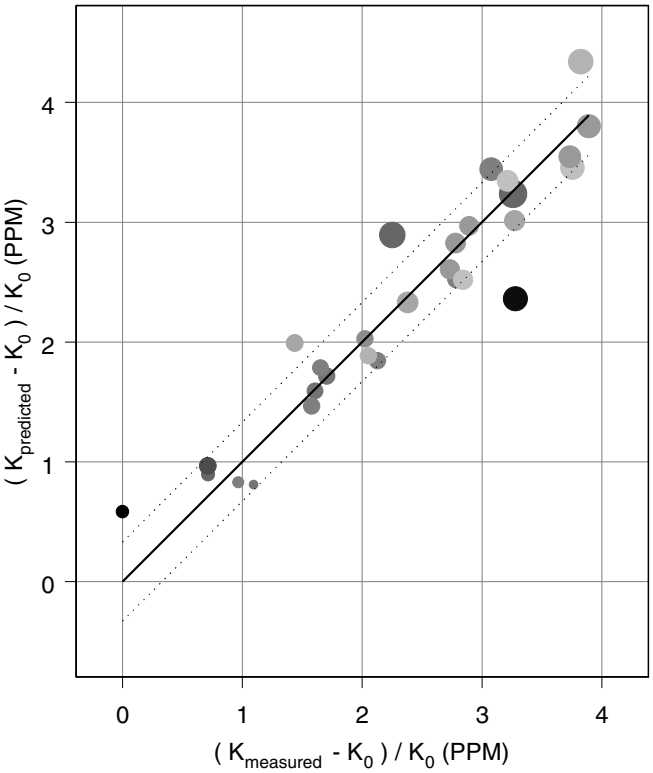

FIG. 3: Global fit to 29 GAMS4 calibrations. Predictions from a five parameter global fit [Eq. (3)] are plotted versus measured calibration values. The standard deviation of the relative residuals given in the last column of Table V is 0.33×10^{-6}. The dotted lines correspond to $\pm 0.33 \times 10^{-6}$ about the fit. Across the data sets the temperature ranges from 25.5 to 26.8 °C corresponding to a 1.9×10^{-6} relative change in K, the relative humidity ranges from 0.21 to 0.58 corresponding to a 3.0×10^{-6} relative change in K, and 4.6 years separates the first and last measurements corresponding to a 2.0×10^{-6} relative change in K. The size of the plotted points is proportional to the humidity while darker (lighter) points represent lower (higher) temperatures.

B. Other Calibration Procedures

For the later measurement cycles, multiple calibrations were performed: ^{33}S 1998 - 4, ^{33}S 1999 - 3 and ^{28}Si 2000 - 5. Since these calibrations were dispersed throughout the measurement cycle, it is possible to interpolate between the measured calibrations using spline fitting to obtain calibration constant values for converting profile data in fringes to angles. This procedure assumes that each of the recorded angle calibrations is valid and the angle cal-

TABLE V: GAMS4 angle calibrations. Each line represents a unique calibration of the spectrometer. Column 1 gives the date of the calibration, column 2 the nuclide being measured, column 3 the calibration-average corner cube arm temperature (°C), column 4 the calibration-average relative humidity, column 5 the measured instrument calibration constant K, column 6 the measured calibration zero, and column 7 the residuals from a five parameter fit to K. The horizontal line indicates the time when the interferometer laser was replaced causing a $(1.22 \pm 0.22) \times 10^{-6}$ one time fractional shift in K. "CC" denotes corner cube.

Date	Nuclide measured	Avg CC arm temp (°C)	Avg relative humidity	K	f_0	Fit rel dev$\times 10^6$
09/27/1997	^{36}Cl	25.595	0.495	5133471.3	588.3	−0.92
03/08/1998		26.272	0.317	5133463.2	−747.7	0.01
03/26/1998		26.266	0.209	5133460.1	−721.1	−0.28
03/30/1998		26.256	0.308	5133462.7	−721.2	−0.01
09/26/1998	^{33}S	26.716	0.481	5133473.7	−547.5	−0.30
10/21/1998	^{33}S	26.607	0.323	5133461.8	−547.7	0.55
11/05/1998	^{33}S	26.308	0.314	5133462.6	−203.1	−0.11
11/17/1998	^{33}S	26.199	0.265	5133458.1	−202.9	0.18
04/13/1999	^{33}S	26.041	0.323	5133458.1	−186.9	0.25
04/30/1999	^{33}S	26.194	0.536	5133466.0	−186.9	0.64
05/07/1999	^{33}S	26.173	0.583	5133471.2	−68.2	−0.02
09/17/1999		26.492	0.464	5133474.4	−268.2	−0.09
09/19/1999		26.486	0.434	5133473.6	−268.1	−0.18
09/25/1999		26.648	0.503	5133474.1	−255.5	0.52
10/05/1999		26.354	0.334	5133468.8	−254.5	−0.26
10/15/1999		26.348	0.449	5133470.3	−249.5	0.37
10/18/1999		26.477	0.369	5133469.3	−249.4	0.08
12/03/1999		25.493	0.257	5133454.5	−249.5	0.59
07/06/2000		26.545	0.399	5133471.3	−183.5	−0.26
07/18/2000		26.474	0.390	5133468.7	−183.4	0.05
10/15/2000	^{29}Si	26.779	0.412	5133471.0	−253.2	0.13
10/22/2000	^{29}Si	26.490	0.374	5133468.5	−192.4	−0.12
11/05/2000	^{29}Si	26.313	0.314	5133465.4	−240.8	−0.28
11/14/2000	^{29}Si	26.409	0.320	5133464.8	−262.2	0.00
11/28/2000	^{29}Si	26.302	0.312	5133462.9	−276.1	0.14
10/28/2001		26.725	0.374	5133469.1	−211.8	−0.32
11/06/2001		26.619	0.316	5133465.0	−250.0	−0.16
11/12/2001		26.347	0.236	5133459.4	−250.0	−0.13
05/19/2002		26.551	0.411	5133466.7	−263.4	−0.05

ibration varies smoothly with time during the measurement cycle. Although the individual calibration values within a measurement cycle are dependent on temperature, humidity, and day number, the spline fitting uses only the individual calibration values and assumes no explicit dependence on temperature, humidity or day number. We have called this calibration procedure the Spline Calibration. It uses only the calibration information obtained during a given measurement cycle to analyze the wavelength data recorded in that cycle. The ^{33}S and ^{29}Si data were analyzed using the spline calibration and the relative difference between wavelengths obtained with the global and spline calibration procedures is $\approx 0.2 \times 10^{-6}$. Since only one calibration was recorded during the ^{36}Cl 1997 measurement cycle, the spline calibration could not be applied to this data. This led us to a third calibration procedure called the Local-Global Calibration.

In the local-global calibration, the calibrations that were performed in a particular measurement cycle are given a more significant role in the determination of $K(\vartheta, d, h)$ for that measurement cycle. First, K_ϑ, K_d, K_h, and $K_{\rm laser}$ are taken as given in Eq. (4) since these coefficients are not expected to change with time and a global fit provides the best estimate of these coefficients. Next the subset of calibrations performed in each measurement cycle are fit to the equation

$$\begin{aligned} K = \quad & K_0 + 7.5(\vartheta - 26) - 0.0059(d - 800) \\ & + 41.6(h - 0.35) + 3.13 \times \begin{cases} -1 & \text{if } d < 700, \\ 1 & \text{if } d > 700 \end{cases} \end{aligned} \quad (5)$$

to obtain independent values of K_0 for each measurement cycle. All of the ^{33}S and ^{29}Si data were analyzed using the local-global calibration procedure and the relative difference between wavelengths obtained with global and local-global calibration procedures is $\approx 0.3 \times 10^{-6}$. The ^{36}Cl data were also analyzed using the local-global calibration procedure and show significantly larger relative differences ($\approx 0.9 \times 10^{-6}$) between wavelengths obtained with the global and local-global calibration procedures. These large differences result from recording only one calibration during the ^{36}Cl measurement cycle and from the fact that this particular calibration is the most discrepant point in the global fit of Fig. 3.

Consideration of these alternate calibration procedures did not provide sufficient evidence to make a "best" calibration procedure choice. All of the wavelength and energy values reported in this paper were obtained using the global calibration procedure. Our reasons for choosing this procedure are 1) all of the available data can be analyzed using one procedure and 2) this procedure makes the maximum use of the available calibration data.

C. Calibration Uncertainty

Although consideration of three calibration procedures did not lead to a clear "best" procedure, this exercise does provide an estimate of the calibration uncertainty. The variation of wavelengths obtained with the global, spline and local-global calibration procedures suggests a relative calibration uncertainty of 0.2–0.3 $\times 10^{-6}$. A second estimate of the calibration uncertainty is available from the fit used in the global calibration procedure. The standard deviation of the relative residuals given in Table V and shown in Fig. 3 is 0.33×10^{-6} and provides a measure of the quality of the fit and the uncertainty of this calibration procedure. A third estimate of the calibration uncertainty is the variation of the wavelength values obtained in different measurement cycles. In this approach lower energy (larger angles) intense transitions must be used because higher energy (smaller angles) weak transitions have a statistical uncertainty that masks the calibration uncertainty. The 841 keV line in ^{33}S was measured in 1998 and 1999 and shows a relative excess variation of 0.38×10^{-6} if the global calibration procedure is used and 0.16×10^{-6} if the spline calibration is used. In addition, this instrumental set up was used to measure an intense line that does not contribute to the binding energy determinations presented here, namely the 816 keV line in ^{168}Er. This line was measured in two different measurement cycles, Oct-Nov 2000 and Nov 2003 and shows a relative excess variation of 0.45×10^{-6} and 0.3×10^{-6} for the global and spline calibrations, respectively. Although it is difficult to obtain a rigorous calibration uncertainty from these three estimates, we choose to use the above values to arrive at a slightly conservative relative calibration uncertainty of 0.4×10^{-6}. This calibration uncertainty will be combined with the statistical and other systematic uncertainties to obtain final wavelength uncertainties.

V. WAVELENGTH MEASUREMENTS

Wavelengths are determined by combining a sequence of profile angle measurements. First the profile centroids and uncertainties in interferometer fringes are converted into angles via Eq. (2). The calibration constant K that appears in this equation has been appropriately corrected for the corner cube arm temperature, the relative humidity, and time. Each of these angles is next corrected for vertical divergence as discussed in Ref. 23. Typically these corrections are between 2 and 4×10^{-7} in relative size. For a given energy and configuration the profiles are recorded with the first crystal in a fixed position and the second crystal sequentially in a more and less dispersive position (see Fig. 2). In addition, the data recording sequence includes both cw and ccw rotation of the second crystal. To more concretely illustrate how wavelengths are determined, we use the ^{33}S 841 keV (1,−3), (1,3) measurement as an example. A group of four profiles recorded in the sequence (1,−3 cw), (1,3 cw), (1,3 ccw), (1,−3 ccw) is used to determine a wavelength value. The four angles associated with the four profiles are fit with the equation

$$\theta(n,t,\vartheta) = \arcsin\left(\frac{n\lambda_{\rm meas}}{2d(\vartheta)}\right) + \theta_0(t)\,, \qquad (6)$$

where n is the diffraction order, t is the time, ϑ is the crystal temperature, $\lambda_{\rm meas}$ is the sought after wavelength, $d(\vartheta)$ is the lattice spacing at crystal temperature ϑ and $\theta_0(t)$ represents the potentially time dependent angular offset between the second crystal diffracting planes and the angle interferometer. The symbol $\lambda_{\rm meas}$ is introduced to indicate that wavelengths determined using this equation are laboratory measured wavelengths (not corrected for recoil); $d(\vartheta)$ is given by

$$d(\vartheta) = d_{22.5\ ^\circ{\rm C},\ {\rm atm}}(1 + 2.56 \times 10^{-6}(\vartheta - 22.5))\,, \qquad (7)$$

where $d_{22.5\ ^\circ{\rm C},\ {\rm atm}}$ is the lattice spacing at 22.5 °C and atmospheric pressure. The lattice parameter measurements given in Table IV are specified for vacuum. To obtain the value at the pressure present in the reactor hall ($p \approx 0.987$ atmospheres) it is necessary to use the following transformation

$$d_{22.5\ ^\circ{\rm C}}(p) = d_{22.5\ ^\circ{\rm C},\ {\rm vac}}(1 - \epsilon p)\,, \qquad (8)$$

where p is the pressure. In this equation $\epsilon = 0.3452 \times 10^{-6}$/atmosphere [24, 25].

In the fit to Eq. (6), the three parameters are the wavelength, a constant angular offset, and a linear temporal offset term (i.e., $\theta_0(t) = a + bt$). Each of the four angles θ_i is weighted by $(1/\sigma_{\theta_i})^2$ where σ_{θ_i} is the profile centroid uncertainty. This sequence of profiles is repeated multiple times in at least two different sets of orders (here 29

instances of (1,−3), (1,3); 21 instances of (1,−1), (1,1); and 1 instance of (1,−3), (1,−1), (1,1), (1,3)). An uncertainty equal to the standard deviation of the wavelength determinations in a unique set of orders is assigned to each wavelength determination derived from that set of orders. The average wavelength is the weighted mean of all the individual determinations. We find no evidence for an order dependent effect in the wavelength data.

Table VI gives the nuclide, the nominal energy, the crystals, the total number of Bragg angle measurements and mean wavelength along with the statistical uncertainties in parentheses. The sulfur transitions appear twice because they were measured in 1998 and 1999.

In Table VII, final measured wavelength values and uncertainties are reported (column 3). Four additional sources of uncertainty have been added in quadrature to the statistical uncertainties given in Table VI. These are the calibration uncertainty discussed in Sec. IV and uncertainties associated with the crystal temperature, the vertical divergence of the gamma-ray beam, and the measured lattice spacing. A relative calibration uncertainty of 0.4×10^{-6} is applied to each energy listed in Table VI. To obtain final sulfur wavelengths and uncertainties it is necessary to add the calibration and statistical uncertainties in quadrature for each sulfur transition before statistically combining the 1998 and 1999 values. This has the effect of reducing the calibration uncertainty for the sulfur lines because they were measured twice. In the case of binding energies where one sums transition energies, the calibration uncertainty is applied to the sum rather than to the constituent transitions; and again, two binding energies are combined to arrive at a final sulfur binding energy. The other three uncertainties are applied to the final transition energies or to the binding energies. An uncertainty in the crystal temperature measurement of 0.05 °C contributes a relative uncertainty of 0.1×10^{-6}. The vertical divergence uncertainty accounts for the possible misalignment of the gamma-ray beam with respect to the plane of dispersion of the spectrometer. A misalignment of 5 mm over a distance of 15 m leads to a relative wavelength uncertainty of 0.06×10^{-6}. This uncertainty is approximately 20% of the size of the correction. From Sec. III C and Table IV, the relative crystal lattice spacing uncertainty is 0.05×10^{-6}.

VI. BINDING ENERGY MEASUREMENTS

In column 4 of Table VII the corresponding energy equivalent values $E_{\rm meas}$ are given, where the conversion factor $1\,{\rm m}^{-1} = 1.23984191(11) \times 10^{-6}$ eV was used [2].

The measured wavelength values must be corrected for recoil to obtain wavelength values $\lambda_{\rm trans}$ whose corresponding energies can be summed to obtain binding energies S_n. To excellent approximation we account for the recoil by the transformation

$$\frac{hc}{\lambda_{\rm trans}} = \frac{hc}{\lambda_{\rm meas}} + \frac{1}{2Mc^2}\left(\frac{hc}{\lambda_{\rm meas}}\right)^2 , \qquad (9)$$

where M is the mass of the decaying nucleus, h is the Planck constant, and c is the speed of light. The second term in Eq. (9) accounts for the loss of energy imparted to the recoiling nucleus. If the decay occurs in flight, there will be a first order Doppler effect. It causes no shift in the central value as long as the motion is isotropic as is expected to be the case here. As discussed in Ref. 26, two additional terms appear in Eq. (9) in the case of decays from the capture state. First, the kinetic energy of the incident neutron ($\approx 0.057\,{\rm eV}$) must be subtracted from the measured gamma-ray energy. For the three capture gamma-rays measured here (3539 keV in ^{29}Si, 5421 keV in ^{33}S, and 6111 keV in ^{36}Cl), this effect is less than 0.02×10^{-6}. Second, there is a Doppler term if the incident neutron comes from a particular direction. The relative peak-to-peak amplitude of this term is $\approx 0.6 \times 10^{-6}$ for the nuclei being discussed here. The term vanishes if the incident neutron direction is isotropic as is expected to be the case here. The relative uncertainty of the recoil correction is estimated to be no greater than 0.01×10^{-6}. As such it is negligible given the current accuracy of $\lambda_{\rm meas}$. Values for $\lambda_{\rm trans}$ and the corresponding energy equivalent $E_{\rm trans}$ are given in Table VII, column 5 and 6.

To obtain a wavelength equivalent to the binding energy, $\lambda_{\rm be}$, we sum the reciprocals of the $\lambda_{\rm trans}$ values for the transitions comprising the binding energy cascade and then convert $\lambda_{\rm be}$ into atomic mass units using the conversion factor: $1\,{\rm m}^{-1} = 1.3310250506(89) \times 10^{-15}$ u [2]. Likewise, the binding energy can be expressed in eV by using the ${\rm m}^{-1}$ to eV conversion factor given above. Table VIII contains values for the three binding energies of ^{29}Si, ^{33}S, and ^{36}Cl in meters, atomic mass units and electron volts.

VII. DISCUSSION

In this section we discuss the consistency of gamma-ray based and atomic mass based binding energy measurements and compare the gamma-ray measurements reported here with other high precision gamma-ray measurements. As discussed in Sec. I, precision atomic mass measurements can be used to determine binding energies. By using atomic mass values from the Atomic Mass Data Center [27, 28] and the fundamental constants [2] along with Eq. (1), binding energies primarily based on atomic mass measurements can be determined. However, since the determination of the neutron mass includes a gamma-ray measurement, binding energy determinations based on Eq. (1) are a combination of atomic mass measurements and gamma-ray measurements. This difficulty can be circumvented by expressing $m(n)$ in terms of m(H),

TABLE VI: Values of the measured wavelengths for the transitions included in the binding energy determinations. The uncertainties are statistical only.

Nuclide	Energy (keV)	Crystals	Number of Bragg angle measurements	$\lambda_{\rm meas} \times 10^{12}$ (m)	relative uncertainty $\times 10^6$
^{29}Si	3539	ILL4.4&6.9	42	0.350340126(44)	0.13
	4934	ILL4.4&6.9	147	0.25128808(18)	0.70
^{33}S	841[a]	ILL2.5	26	1.47429306(14)	0.09
	2380[a]	ILL2.5	18	0.52103852(30)	0.58
	5421[a]	ILL4.4&6.9	42	0.228730970(63)	0.27
	841[b]	ILL2.5	25	1.47429225(12)	0.08
	2380[b]	ILL2.5	31	0.52103905(23)	0.43
	5421[b]	ILL4.4&6.9	30	0.22873089(13)	0.56
^{36}Cl	517	ILL2.5	15	2.39782393(10)	0.04
	786	ILL2.5	2	1.57681233(83)	0.53
	1951	ILL2.5	12	0.63544928(10)	0.16
	6111	ILL2.5, ILL4.4&6.9	17	0.20288757(10)	0.50

[a]Sept–Oct 1998
[b]April–May 1999

TABLE VII: Measured and recoil corrected (transition) wavelengths and energies. Measured values from Ref. 6 for ^{2}H, which have been adjusted for the adjusted value of d(220) ILL2.5, are included for convenience.

Nuclide	Energy (keV)	$\lambda_{\rm meas} \times 10^{12}$ (m)	$E_{\rm meas}$ (eV)	$\lambda_{\rm trans} \times 10^{12}$ (m)	$E_{\rm trans}$ (eV)	wavelength relative uncertainty $\times 10^6$
^{29}Si	3539	0.35034013(15)	3538966.3(1.6)	0.35031716(15)	3539198.3(1.6)	0.44
	4934	0.25128808(21)	4933946.3(4.0)	0.25126511(20)	4934397.4(4.0)	0.82
^{33}S	841	1.47429265(47)	840974.08(28)	1.47427246(47)	840985.60(28)	0.32
	2380	0.52103883(24)	2379557.6(1.1)	0.52101864(24)	2379649.8(1.1)	0.47
	5421	0.228730944(95)	5420525.5(2.3)	0.228710758(95)	5421003.9(2.3)	0.42
^{36}Cl	517	2.3978239(10)	517069.62(22)	2.3978054(10)	517073.61(22)	0.42
	786	1.5768123(11)	786296.43(53)	1.5767938(11)	786305.66(53)	0.67
	1951	0.63544928(29)	1951126.47(89)	0.63543077(29)	1951183.30(89)	0.45
	6111	0.20288757(13)	6110980.2(4.0)	0.20286906(13)	6111537.6(4.0)	0.66
^{2}H	2223	0.557671328(99)	2223248.44(44)	0.557341007(99)	2224566.10(44)	0.18

TABLE VIII: Measured binding energies in meters (m), atomic mass units (u) and electron volts (eV). $\lambda_{\rm be} = \frac{1}{\sum_i \frac{1}{\lambda_{{\rm trans}_i}}}$ is the wavelength of a photon whose energy is equal to the binding energy. Measured values from Ref. 6 for ^{2}H, which have been adjusted for the adjusted value of d(220) ILL2.5, are included for convenience.

Nuclide	$\lambda_{\rm be} \times 10^{12}$ (m)	$S_n \times 10^3$ (u)	S_n (eV)	wavelength relative uncertainty $\times 10^6$
^{29}Si	0.146318275(86)	9.0967793(53)	8473595.7(5.0)	0.59
^{33}S	0.143472991(54)	9.2771820(35)	8641639.8(3.3)	0.38
^{36}Cl	0.144507180(80)	9.2107883(51)	8579794.5(4.8)	0.55
^{2}H	0.557341007(98)	2.38816996(42)	2224566.10(44)	0.18

$m(^2\mathrm{H})$ and $S_n(^2\mathrm{H})$. By making this substitution and rearranging terms, Eq. 1 becomes

$$m(^A\mathrm{X}) - m(^{A+1}\mathrm{X}) + m(^2\mathrm{H}) - m(\mathrm{H}) = S_n(^{A+1}\mathrm{X}) - S_n(^2\mathrm{H})\,. \qquad (10)$$

Since the left and right sides of this equation involve only atomic mass and gamma-ray measurements respectively, this equation is a valid test of the consistency of high-precision atomic mass and gamma-ray measurements.

Recently, new highly accurate values for the left hand side of this equation have been reported for $^{A+1}$X equal to ^{29}Si and ^{33}S [29]. In these measurements the cyclotron frequencies of two different ions simultaneously confined in a Penning trap were directly compared. The measured quantities are the mass ratios $m[^{33}\mathrm{S}^+]/m[^{32}\mathrm{SH}^+]$ and $m[^{29}\mathrm{Si}^+]/m[^{28}\mathrm{SiH}^+]$ from which, along with the quantity $m(^2\mathrm{H})-2m(\mathrm{H})$, the mass differences on the left hand side of Eq. 10 are derived. In Table IX, column 2 the left hand side mass differences for Si and S are given. The relative uncertainties for the Si and S values in column 2 are 7.0×10^{-8} and 7.3×10^{-8} respectively.

Values for the right hand side of this equation for $^{A+1}$X equal to ^{29}Si and ^{33}S follow directly from the binding energies given in Table VIII and are given in Table IX, column 3. The relative uncertainties for the Si and S values in column 3 are 8.0×10^{-7} and 5.1×10^{-7} respectively.

In Fig. 4 the values given in Table IX are plotted to show the consistency of the atomic mass and gamma-ray measurements. The left and bottom axes are used for ^{29}Si, while the top and right axes are used for ^{33}S. The scales of the axes have been chosen so that a diagonal line through the plot represents exact consistency between atomic mass and gamma-ray measurements. The plot shows that the quality of the consistency test is limited by the uncertainty of the gamma-ray measurements. For ^{29}Si the two measurements are slightly inconsistent ($1.2\,\sigma$), while for ^{33}S the two measurements agree within the uncertainty ($0.4\,\sigma$).

In Table IX, column 4 the fractional difference between the atomic mass and gamma-ray measurements is given along with the weighted average of the Si and S fractional differences. These measurements confirm the consistency of atomic mass and gamma-ray measurements with a relative uncertainty of 4.3×10^{-7}.

The most accurate Si and S gamma-ray energies were measured using Ge(Li) solid state spectrometers. These spectrometers derive an energy scale from gamma-ray standard energies. For high precision comparisons, the published values of the gamma-ray energies need to be adjusted to account for changes in the energy standards. Because a number of energy standards covering a wide energy range are used, the shift in the energy scale for a particular energy is difficult to estimate. Although the procedure that has been used is not rigorous, it is likely sufficient given the accuracy of the published energies. New values for the standards were taken from Ref. 30 or have been determined using atomic mass values from Refs. 2, 27, and 28. For ^{29}Si the values of the 3539 keV and the 4945 keV energies in Ref. 31 have been corrected by -7 eV to account for the change in the 2223 keV and the 4945 keV standards produced in the $^1\mathrm{H}(n,\gamma)$ and $^{12}\mathrm{C}(n,\gamma)$ reactions, respectively. For ^{33}S the values for the 841 keV, 2380 keV, and 5421 keV energies in Ref. 32 have been corrected by $+8$ eV, -107 eV, and -107 eV respectively. These corrections account for changes in the 412 keV standard produced in the decay of ^{198}Au and changes in the 2223 keV, the 4945 keV, and the 10829 keV standards produced in the $^1\mathrm{H}(n,\gamma)$, the $^{12}\mathrm{C}(n,\gamma)$, and the $^{15}\mathrm{N}(n,\gamma)$ reactions, respectively. For the low energy Cl lines considerably more precise data exists. In 1985 energy values for some Cl lines were measured using the GAMS4 facility in its early stage of development [33]. These published values also need to be corrected for changes in the fundamental constants [2] and known errors in the lattice spacing of the crystals [34]. These corrections to the Cl lines can be made with much more certainty than the corrections to the ^{29}Si and ^{33}S lines.

In Table X we compare the E_{meas} values in this report (column 2) with the corrected E_{meas} values from other references (column 3). For the ^{29}Si and ^{33}S gamma-rays the new measurements agree with the corrected older measurements within the uncertainty except for the 5421 keV line which differs by 1.3 times the combined uncertainty. Because of the large uncertainty of the older Si and S measurements, this comparison does not provide a very stringent test of our new measurements. However, the consistency of the Cl measurements over more than 15 years during which the spectrometer, the crystals, and measurement procedures were significantly changed lends a large measure of confidence to the gamma-ray measurements.

Acknowledgments

We thank Albert Henins for preparing the diffracting crystals that are used on GAMS4.

[1] R. D. Deslattes and E. G. Kessler, Jr., in *Atomic Masses and Fundamental Constants-6*, edited by J. A. Nolan Jr. and W. Benenson (Plenum Press, New York, 1979), pp. 203–218.

[2] P. J. Mohr and B. N. Taylor, *The 2002 CODATA recommended values of the fundamental physical constants, web version 4.0*, available at physics.nist.gov/constants (National Institute of Standards and Technology, Gaithersburg, MD 20899, 9 December 2003).

[3] M. A. Lone, R. A. Leavitt, and D. A. Harrison, Atomic

TABLE IX: Consistency of high precision atomic mass and gamma-ray measurements.

$^{A+1}$X	$m(^{A}\mathrm{X}) - m(^{A+1}\mathrm{X}) + m(^{2}\mathrm{H}) - m(\mathrm{H})$ (u)	$S_n(^{A+1}\mathrm{X}) - S_n(^{2}\mathrm{H})$ (u)	relative difference (col3 − col2)/col3 × 10^7
^{29}Si	0.00670861569(47)	0.00670860929(536)	−9.54(8.02)
^{33}S	0.00688901053(50)	0.00688901206(351)	2.22(5.15)
weighted average			
relative difference			−1.21(4.33)

TABLE X: Comparison of measured gamma-ray energies.

Nuclide	This report E_{meas} (eV)	Other references[a] E_{meas} (eV)
^{29}Si	3538966.3(1.6)	3538973(40)
	4933946.3(4.0)	4933973(30)
^{33}S	840974.08(28)	840982(14)
	2379557.6(1.1)	2379550(11)
	5420525.5(2.3)	5420473(40)
^{36}Cl	517069.62(22)	517070.10(23)
	786296.43(53)	786297.02(39)
	1951126.47(89)	1951127.92(1.37)

[a] ^{29}Si Ref. 31; ^{33}S Ref. 32; ^{36}Cl Ref. 33

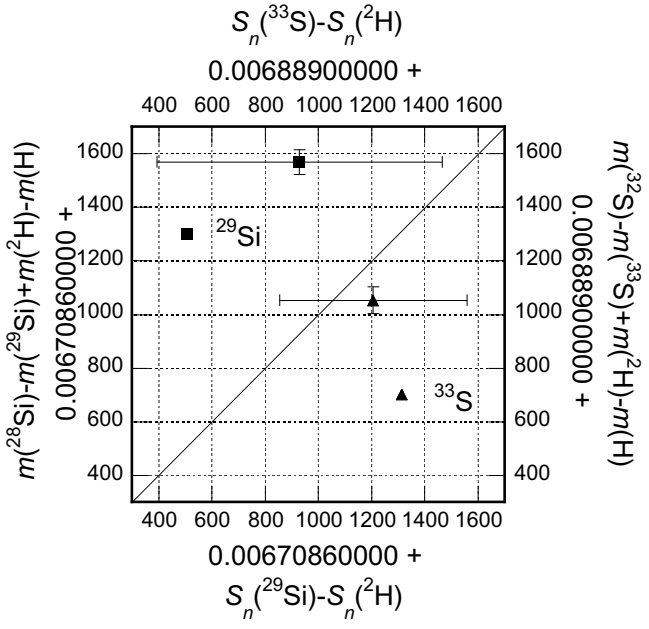

FIG. 4: Mass differences determined in a Penning trap versus those determined from wavelength determinations. The left (right) and bottom (top) axes correspond to Si (S). The scales of the axes have been chosen so that a diagonal line through the plot represents exact consistency between Penning trap and gamma-ray measurements. The plot shows that the quality of the consistency test is limited by the uncertainty of the gamma-ray measurements.

Data and Nuclear Data Tables **26**, 511 (1981).
[4] R. B. Firestone, V. S. Shirley, S. Y. F. Chu, C. M. Baglin, and J. Zipkin, *Table of Isotopes* (John Wiley and Sons, Inc., New York, New York, 1996), eighth ed.
[5] E. G. Kessler, Jr., M. S. Dewey, R. D. Deslattes, A. Henins, H. G. Börner, M. Jentschel, and H. Lehmann, Nucl. Instrum. Methods Phys. Research **A457**, 187 (2001).
[6] E. G. Kessler, Jr., M. S. Dewey, R. D. Deslattes, A. Henins, H. G. Börner, M. Jentschel, C. Doll, and H. Lehmann, Phys. Lett. A **A255**, 221 (1999).
[7] The identification of the supplier of the crystal material is included to more completely describe the experiment. Such identification does not suggest endorsement nor indicate that this material is necessarily best suited for this application.
[8] P. Becker, K. Dorenwendt, G. Ebeling, R. Lauer, W. Lucas, R. Probst, H.-J. Rademacher, G. Reim, P. Seyfried, and H. Siegert, Phys. Rev. Lett. **46**, 1540 (1981).
[9] G. Basile, A. Bergamin, G. Cavagnero, G. Mana, E. Vittone, and G. Zosi, Phys. Rev. Lett. **72**, 3133 (1994).
[10] K. Nakayama and H. Fujimoto, IEEE Trans. Instr. and Meas. **46**, 580 (1997).
[11] D. Windisch and P. Becker, Phys. Status Solidi **118**, 379 (1990).
[12] E. G. Kessler, A. Henins, R. D. Deslattes, L. Nielsen, and M. Arif, Phys. Lett. A **99**, 1 (1994).
[13] E. G. Kessler, J. E. Schweppe, and R. D. Deslattes, IEEE Trans. Instr. and Meas. **46**, 551 (1997).
[14] G. Cavagnero, H. Fujimoto, G. Mana, E. Massa, K. Nakayama, and G. Zosi, Metrologia **41**, 56 (2004).
[15] G. Cavagnero, H. Fujimoto, G. Mana, E. Massa, K. Nakayama, and G. Zosi, Metrologia **41**, 445 (2004).
[16] Private communication, Barry Taylor, NIST.
[17] P. J. Mohr and B. N. Taylor, Rev. Mod. Phys. **72**, 351 (2000).
[18] K. P. Birch and M. J. Downs, Metrologia **30**, 155 (1993), index of refraction stuff.
[19] K. P. Birch and M. J. Downs, Metrologia **31**, 315 (1994), index of refraction stuff.
[20] H. G. Börner and J. Jolie, J. Phys. G: Nucl. Phys. **19**, 217 (1993).
[21] A. Bergamin, G. Cavagnero, G. Mana, and G. Zosi, J. Appl. Phys. **82**, 5396 (1997).
[22] J. W. Berthold and S. F. Jacobs, Applied Optics **15**, 1898 (1976).
[23] H. W. Schnopper, J. Appl. Phys. **36**, 1415 (1965).
[24] J. F. Nye, *Physical Properties of Crystals* (Oxford University Press, Oxford, England, 1957), pp. 146–147.
[25] H. J. McSkimin, J. Appl. Phys. **24**, 988 (1953).
[26] Y. Ko, M. K. Cheoun, and I.-T. Cheon, Phys. Rev. C **59**,

3473 (1999).
[27] *The atomic mass data center*, `http://www.nndc.bnl.gov/amdc/`.
[28] G. Audi and A. H. Wapstra, Nucl. Phys. A **595**, 409 (1995).
[29] Private communication, Professor David E. Pritchard, MIT.
[30] R. G. Helmer and C. van der Leun, Nucl. Instrum. Methods A **450**, 35 (2000).
[31] S. Raman, E. T. Jurney, J. W. Starner, and J. E. Lynn, Phys. Rev. C **46**, 972 (1992).
[32] S. Raman, R. F. Carlton, J. C. Wells, E. T. Jurney, and J. E. Lynn, Phys. Rev. C **32**, 18 (1985).
[33] E. G. Kessler, Jr., G. L. Greene, R. D. Deslattes, and H. G. Börner, Phys. Rev. C **32**, 374 (1985).
[34] R. D. Deslattes, M. Tanaka, G. L. Greene, A. Henins, and E. G. Kessler, Jr., IEEE Trans. Instr. and Meas. **36**, 1660169 (1987).